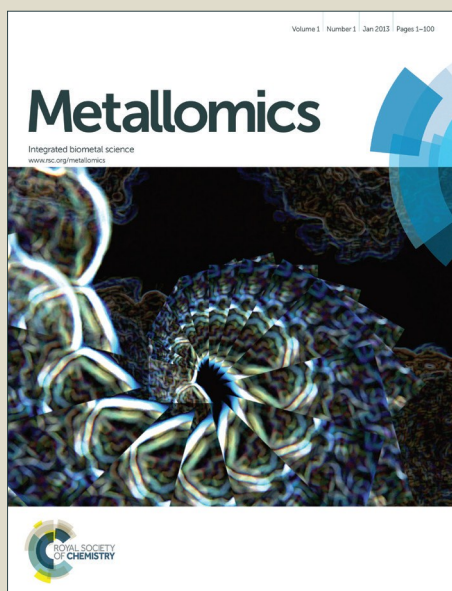


Metallomics

Accepted Manuscript



This is an *Accepted Manuscript*, which has been through the Royal Society of Chemistry peer review process and has been accepted for publication.

Accepted Manuscripts are published online shortly after acceptance, before technical editing, formatting and proof reading. Using this free service, authors can make their results available to the community, in citable form, before we publish the edited article. We will replace this *Accepted Manuscript* with the edited and formatted *Advance Article* as soon as it is available.

You can find more information about *Accepted Manuscripts* in the [Information for Authors](#).

Please note that technical editing may introduce minor changes to the text and/or graphics, which may alter content. The journal's standard [Terms & Conditions](#) and the [Ethical guidelines](#) still apply. In no event shall the Royal Society of Chemistry be held responsible for any errors or omissions in this *Accepted Manuscript* or any consequences arising from the use of any information it contains.

ARTICLE

Quantitative elemental analysis of bovine ovarian follicles using X-ray fluorescence imaging

M.J. Ceko,^a K. Hummitzsch,^b N. Hatzirodos,^b R.J. Rodgers^b and H.H. Harris^a

Cite this: DOI:
10.1039/x0xx00000x

Received 00th June 2014,
Accepted 00th June 2014

DOI: 10.1039/x0xx00000x

www.rsc.org/

The X-ray Fluorescence Micro-spectroscopy (XFM) beamline at the Australian Synchrotron was used to image 97 follicle histological sections from 45 different bovine ovaries focusing on healthy antral follicles ranging from small (< 4 mm) up to preovulatory sizes (> 16 mm) and on antral follicles undergoing atresia. This analysis identified five elements (Cu, Fe, Zn, Se and Br) consistently present within the ovarian tissue with Fe, Zn and Se localised to specific structures. GeoPIXE v6.4g was subsequently used to extract quantitative information pertaining to the elemental concentrations surrounding each of these follicles. Statistical analysis suggested that significant elemental differences were evident between follicle groups sorted according to their health status (Fe and Br), and their size (Se). Se appeared to be the element which most greatly distinguished large antral follicles from smaller counterparts. The ability to use synchrotron radiation to measure trace element distributions in bovine follicles at such high resolutions could have a significant impact on understanding the mechanisms of follicular development. This research is intended to form a baseline study of healthy cycling ovaries which could later be extended to disease states, thereby improving our current understanding of infertility and endocrine diseases involving the ovary.

Introduction

The function of the ovary is to produce and release oocytes to be fertilised, leading to the production of offspring.¹ The adult bovine ovary is a popular experimental model for elucidating mechanisms related to ovarian function in humans owing to structural and physiological similarities between both species' ovaries, and the fact that both species are monovulatory. Follicles are ordinarily categorised according to their stage of growth: primordial follicles; primary follicles; preantral follicles; and, antral follicles having distinct features of their granulosa cells, as well as the formation of a specialised thecal layer at the antral stage, used to differentiate between them. After ovulation of the selected dominant follicle, the remnants of the follicle wall transform into the corpus luteum. During follicular development the vast majority of follicles do not mature to ovulation, but rather regress by an apoptotic process termed atresia.² New technologies, such as synchrotron-based techniques, have the potential to enhance our understanding of ovarian function to the near-cellular level³ and have the advantage of requiring minimal preprocessing of the tissue; thus capturing the distribution of trace elements in the organ as they would have appeared *in vivo*.⁴ Synchrotron light has been rarely used to image ovarian tissue of any species and to our knowledge our work is the first application of X-ray Fluorescence (XRF) imaging to mammalian ovarian tissue.

Of the nine biological trace elements, copper (Cu), iron (Fe), zinc (Zn), and selenium (Se) are important in reproduction in both males and females and the deficiency or excess of these elements can affect both the reproductive organs and overall fertility of an individual.^{5,6} Cu is an essential element required as a functional component of numerous metalloenzymes. Comparisons of Cu concentrations in non-cancerous versus cancerous human ovarian tissues using atomic absorption spectrometry, showed significantly increased Cu concentrations in the cancerous ovarian samples.⁷ A study to investigate the relationship between Fe deficiency and conception outcomes in rats confirmed that Fe deficiency significantly lowered the rate of conception relative to the control group, and also appeared to disrupt the length of the oestrous cycle.⁸ Zn deficiency in females can lead to such problems as: impaired synthesis and/or secretion of follicle stimulating hormone and luteinising hormone; abnormal ovarian development; and, disruption of the oestrous cycle.⁵ In addition, Cu and Zn plasma concentrations have been found to fluctuate throughout the menstrual cycle of healthy women and are correlated with oestradiol levels, suggesting important interplay between these trace elements and female sex hormones.⁹ Several authors have investigated the relationship between Se and fertility, and with regard to ovarian function it has been demonstrated that nutrient restriction and/or Se level in the maternal diet affects cell

proliferation in follicles, blood vessels, and stromal tissues in ovine foetal ovaries.¹⁰ Se deficiency has additionally been shown to lead to degeneration of ovaries and atresia of follicles in rats.¹¹ Finally, potential biological roles of Br based species have been under scrutiny for the past thirteen years with several authors making important contributions to this area of knowledge.¹² A recent ground breaking study has suggested for the first time that Br is actually essential to life. The authors demonstrated an essential role for this element in basement membrane architecture and tissue development, and showed that dietary depletion of Br is lethal in *Drosophila*.¹³

In this research we investigated the accumulation of the trace elements Cu, Fe, Zn, Se and Br in ovarian tissue with a view to investigating whether the elemental distribution can be used to distinguish between antral follicles of different sizes, or between healthy and atretic antral follicles. XRF imaging was used to explore the distribution of these elements in sections of bovine ovarian tissue from 45 different animals which captured portions of 97 antral follicles. Extraction of the elemental concentrations from GeoPIXE v6.4g coupled with statistical analyses indicated that the greatest elemental differences lay in large (10 – 16 mm) and preovulatory (> 16 mm) follicles compared with their smaller counterparts for Se. When grouped according to their health status, the mean elemental concentrations of Br, Fe and Zn could be used to differentiate between early atretic and regressed (Fe), healthy and regressed (Br), and early atretic and regressed (Br) follicles. The ability to probe the in situ bioaccumulation of trace elements to a specific ovarian structure or cell type has the potential to provide unprecedented insights into the biochemistry of this organ.¹⁴

Experimental

Sample collection and preparation for XRF analysis

Bovine ovaries were sourced from T&R Pastoral's abattoir, Murray Bridge, South Australia. Ovaries were collected from non-pregnant heifers (n = 45) and collected in pairs into ice-cold Hank's Balanced-Salt Solution (HBSS) and stored on ice. Sections for XRF imaging were preselected on the grounds that they contained the most structural information and were then frozen in Tissue-Tek[®] OCT compound (ProSciTech Pty Ltd, Thuringowa, QLD, Australia) on dry ice and stored at -80°C until further sectioning.

Each of these ovaries was sectioned at a thickness of 30 µm for XRF imaging with adjacent 6 µm sections taken for haematoxylin and eosin (H&E) staining to subsequently align with XRF data. Sectioning was performed on a CM1800 Leica cryostat (Adeal Pty Ltd., Altona North, VIC, Australia). Each XRF section was supported on Ultralene thin film affixed to a 24 x 36 mm photographic slide frame. Transfer of the section from the cryostat to the thin film was facilitated by a combination of stainless steel tweezers and an artist grade Filbert type synthetic paint brush with care being taken to only touch frozen OCT. Tissue was then desiccator dried under vacuum overnight and stored in a desiccator until synchrotron analysis.

Classification of follicles

Table 1 Classification of antral follicles according to their surface diameter

Classification	Size (mm)
Small	< 4
Small-medium	4-8
Medium-large	8-10
Large	10-16
Preovulatory	> 16

The H&E stains were analysed to determine the health status of the antral follicles as healthy, early atretic, atretic, or regressed. Follicles with greater than 5% apoptotic granulosa cells were classified as early atretic or atretic, and those with less than or equal to 5% apoptotic granulosa cells were designated healthy. In addition, the surface diameter of the follicle was measured and classified as small, small-medium, medium-large, large, or preovulatory according to the values in Table 1.

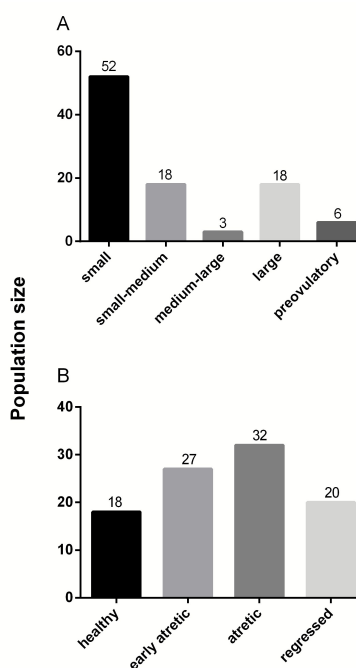


Fig. 1 Population of antral follicles in H&E stained ovarian sections classified by (A) follicle size and (B) health status.

It should be noted that the diameter measuring technique was altered during tissue collection with 87% of the follicles being measured after the tissue was embedded and sectioned, and the remainder being measured upon collection and prior to sectioning. Possible implications of this change in protocol are discussed in *Critique of the analysis*.

ARTICLE

The total cohort consisted of 97 imaged antral follicles with the distribution of follicles across groups being summarised in Fig. 1.

Instrumentation and beamline operating conditions

The distribution of elements throughout selected 30 μm thick bovine ovarian sections was mapped at the XFM beamline at the Australian Synchrotron, Clayton, VIC, Australia. An incident beam of 15.75 keV X-rays was chosen to induce K-shell ionisation of elements with atomic numbers below 37 ($Z \leq \text{Rb}$), while providing adequate separation of the Rayleigh and Compton peaks from the elemental fluorescence of interest, i.e. Se and Br. The incident beam was focused to a $\sim 2 \mu\text{m}$ spot for all scans (full-width at half maximum) using a Kirkpatrick–Baez mirror pair and specimens were fly-scanned through X-ray focus with either a 2 (fine scan) or 6 μm (coarse scans) vertical step size. The resulting XRF was collected in event-mode using the low-latency, 384-channel Maia XRF detector (positioned in the backscatter geometry) and the full XRF spectra used to reconstruct elemental maps of the specimen using a virtual pixel size of 2 or 6 μm (fine and coarse scans, respectively). The effective per pixel dwell times for the fine and coarse scans were 7.81 ms or 2.92 ms, respectively. Single element foils of Mn and Pt (Micromatter, Canada), were scanned in the same geometry and used as references to establish elemental quantitation. Deconvolution of the Maia data was performed using GeoPIXE v6.4g (CSIRO, Australia) that incorporates a linear transformation matrix to perform spectral deconvolution.¹⁵ Spectra were calibrated using the metal foil measurements, and corrections made for self-absorption in the sample, absorption in air, and the efficiency response of the detector.¹⁶ The detected X-ray photons from each pixel were related to calculated-model fluorescence X-ray yields for an assumed specimen composition and thickness. The composition and thickness of the Ultralene film was known from the manufacturer's specifications and the composition and average density typical of dried organic material ($\text{C}_{22}\text{H}_{10}\text{N}_2\text{O}_4$ and 1.42 g cm^{-3} respectively), was used to model the tissue. Absorption effects for XRF from the lowest atomic number element relevant to this study (Ca $K\alpha$) were negligible for this specimen type.

Quantitative analysis within GeoPIXE v6.4g

In order to quantitatively compare trace elemental concentrations across antral follicles any XRF image which captured an entire follicle, or a portion thereof, was included for analysis. In all cases the image regions analysis tool was used within GeoPIXE to obtain average elemental concentrations in regions of interest (ROI) which represented a portion of the follicle circumference. It should be noted that in the majority of cases the coarse nature of

the scans did not provide sufficient resolution to deduce whether the granulosa and thecal cell layers were being exclusively selected. Thus, the portion of the follicle wall selected in each case was intentionally thick enough to incorporate the membrana granulosa, theca interna, theca externa and in some cases a small portion of the adjacent stromal tissue (ranging from 100 μm to 350 μm). For the elements Br, Cu, Fe, Se and Zn, average elemental concentrations (reported in ppm) were exported into Microsoft Excel. Some follicles showed evidence of other trace elements including cobalt (Co), chromium (Cr), manganese (Mn), nickel (Ni), and titanium (Ti) but as these were not in particularly high concentrations, nor were they found in a significant portion of samples ($\leq 10\%$), these elements were excluded from subsequent analysis. In order to minimise artificial elevation of elements due to density effects, the Compton map was used to guide selection of the tissue. More specifically, regions where the tissue may have folded in on itself, or regions where bubble artefacts appeared as a result of the vacuum drying process, were excluded from selection.

Statistical analysis of data

All statistical calculations were performed using Microsoft Excel 2010. For the elemental concentrations between follicle groups, results are presented as means \pm standard error of the mean (SEM). To compare the elemental concentrations between follicle groups (differentiated by both size and state of health), a one way ANOVA with post hoc t-tests was employed and a Bonferroni corrected value of $p < 0.005$ was considered statistically significant. When analysing the Cu concentrations between different follicle groups the F value was less than F_{critical} in both size and health status comparisons. Thus the results were deemed to be not significant at the 5% confidence level and this element has been excluded from further discussion. Principal Component Analysis (PCA) of the data was carried out in The Unscrambler X 10.1.0 (CAMO Software, Oslo, Norway).

Results and discussion

Figure 2 shows histological and XRF elemental distribution images for a representative from the set of bovine ovary sections studied here. Further examples are available in references 12, 14 and 17.

One way analysis of variance (ANOVA) in Excel

One way ANOVA analyses were conducted for each of Fe, Zn, Se and Br within each of the two follicle classifications, size and health status. The analysis of follicles sorted into

size groups showed a significant difference in the level of Se. Bonferroni corrected post hoc t-tests (two sample assuming equal variances, $\alpha = 0.05$) enabled these statistically significant differences to be elucidated to small versus large, and small versus preovulatory follicles (Fig. 3).

When the follicles were sorted according to their health status, significant elemental differences were seen in Fe (early atretic versus regressed), and Br (healthy versus regressed and early atretic versus regressed) (Fig. 4).

For the health status classified Fe analysis, the F value was found to be greater than $F_{critical}$ but application of the conservative Bonferroni correction to the post hoc t-Tests produced only one statistically significant difference (i.e. p exceeded 0.005). The general trend however was for Fe levels to decline as follicles progressed from early atretic through to regressed.

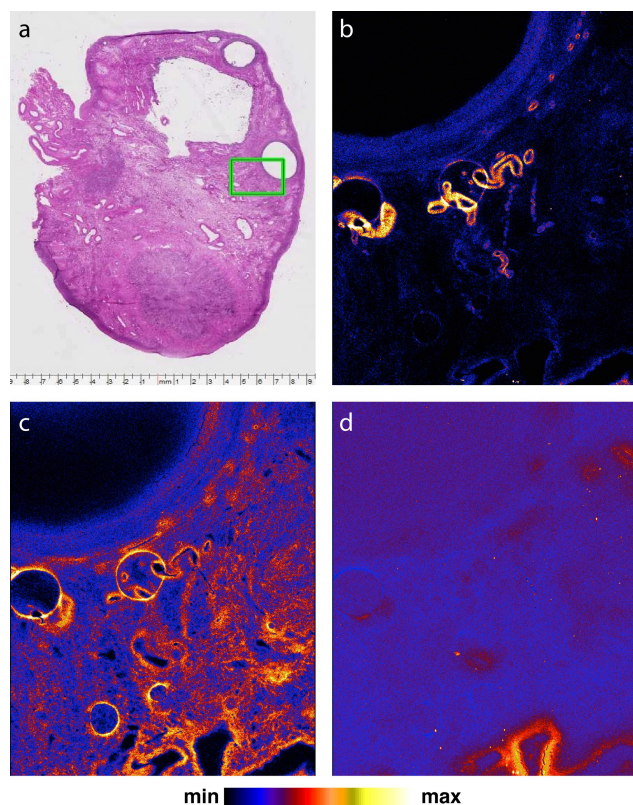


Fig. 2 Representative images of bovine ovary sections. **a**: hematoxylin and eosin stained section (approximate width 18 mm) of entire ovary showing the area imaged using XRF in green; XRF images of a 30 μm thin section adjacent to **a** (rotated 90°), showing the elemental distributions of Zn (**b**), Br (**c**) and Fe (**d**) across the boundary of an antral follicle.

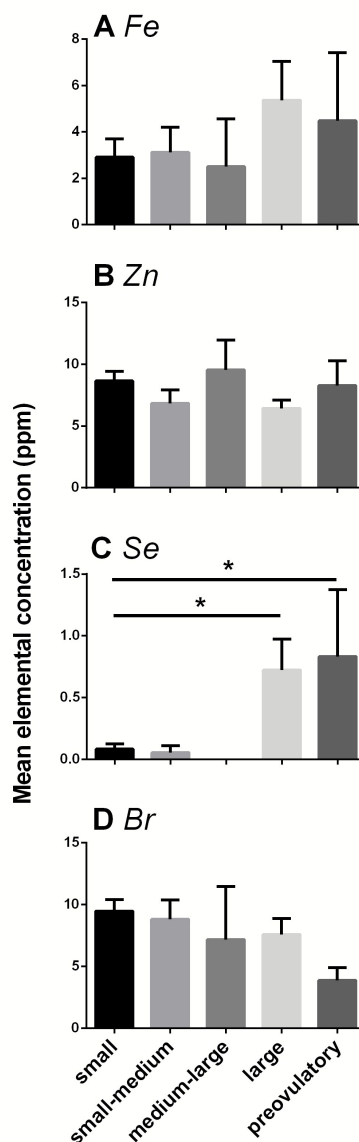


Fig. 3 Summary of mean elemental concentrations (\pm SEM) of (A) Fe, (B) Zn, (C) Se, and (D) Br in antral follicles classified by size as imaged by XRF μ -spectroscopy. *denotes statistically significant differences between groups at each end of the bar $p < 0.005$ (Bonferroni corrected)

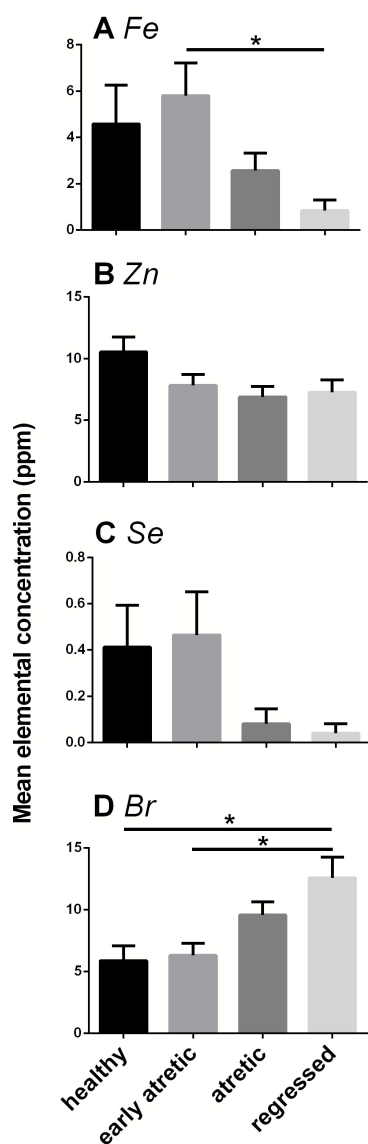


Fig. 4 Summary of mean elemental concentrations (\pm SEM) of (A) Fe, (B) Zn, (C) Se, and (D) Br in antral follicles classified by health status as imaged by XRF μ -spectroscopy. *denotes statistically significant differences between groups at each end of the bar $p < 0.005$ (Bonferroni corrected)

It should be noted that the ovary collection and dissection was carried out in two separate sets with the latter 15% of follicles being measured prior to dissection, and prior to the extraction of follicular fluid. This cohort also

predominantly consisted of large and preovulatory follicles to address this gap in the first cohort. With regard to size classifications in the original cohort, diameter measurements were based on the H&E stained sections following embedding and sectioning. In reality these measurements would represent the minimum diameter the follicle would have had. Thus there could be some overlap between size classified follicle groups and this is reflected by the fact that no statistically significant differences were seen for any elements when comparing small versus medium-large, small-medium versus large, medium-large versus preovulatory antral follicles, nor any other pair of adjacent size groups.

Principal component analysis (PCA) in The Unscrambler X 10.0.1

PCA was conducted on the entire follicle cohort for the elements Fe, Zn, Se and Br. Score plots of PC2, PC3 and PC4 versus PC1 were produced and sample grouping enabled follicles of different sizes, and then at different stages of growth or atresia to be visualised. Although this analysis did not produce any remarkable insights into the data, it did support the statistical conclusion that the trace element composition of large antral follicles differs significantly from that of all other sizes, owing mainly to the presence of Se (Fig. 5). Fig. 6 also provides evidence that healthy and early atretic follicles, irrespective of their size, show similarities in their trace element composition. This is likely due to high structural similarities between these two states and the limitations of classifying follicles based on the H&E stains. Table 2 suggests that the Br data most significantly contributed to PC1, with Fe and Zn heavily contributing to PC2. PC3 consists almost entirely of the Zn data not captured in PC2, and finally, PC4 is almost entirely loaded onto by the Se data.

Table 2 Summary of PC loadings for covariance matrix

Component	Fe	Zn	Se	Br
PC1	-0.389	0.198	-0.021	0.900
PC2	0.850	0.451	0.039	0.269
PC3	-0.352	0.870	-0.021	-0.344
PC4	-0.048	0.005	0.999	0.001

ARTICLE

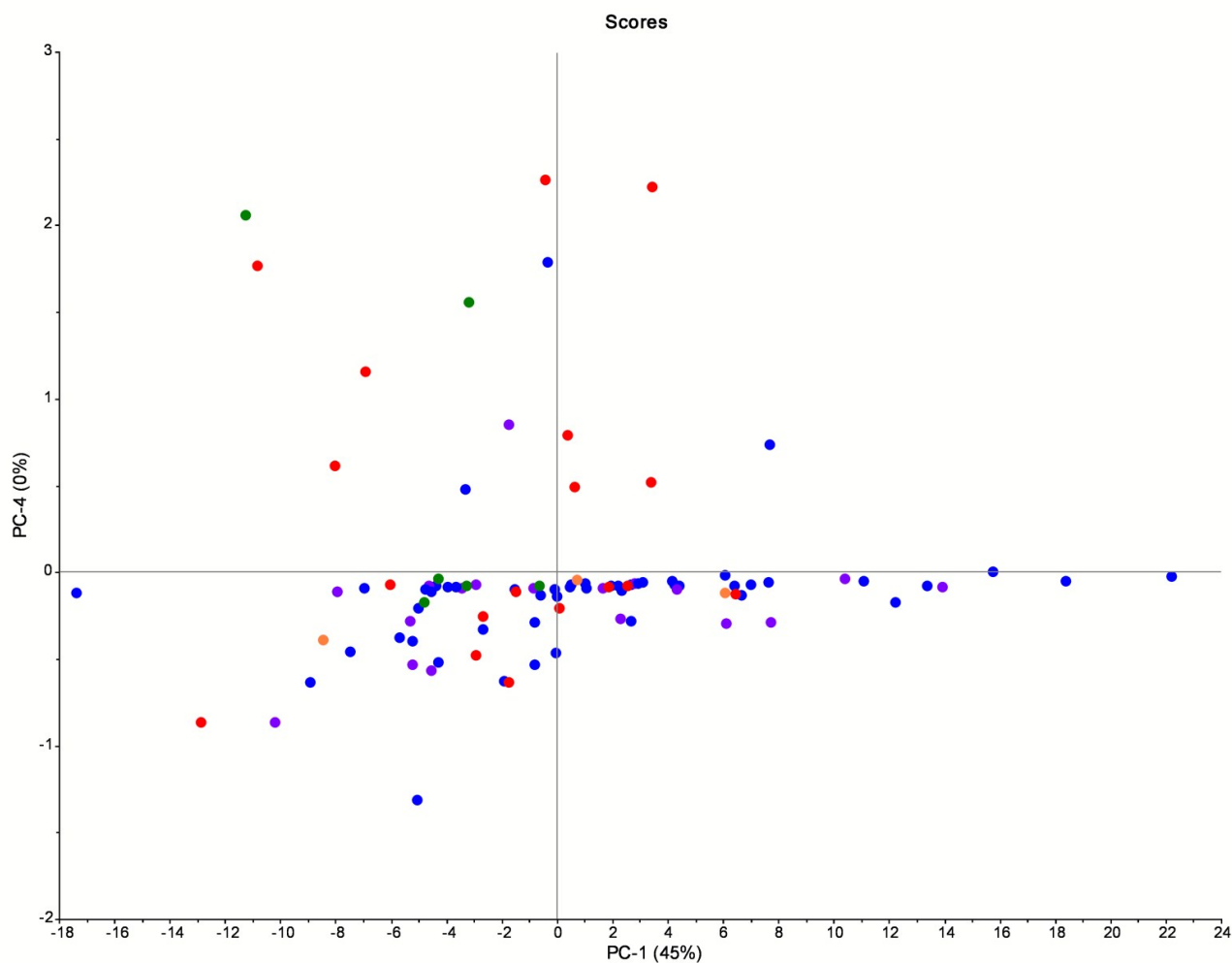


Fig. 5 PC4 versus PC1 scores plot derived from average elemental concentrations data. Follicle health statuses are highlighted in different colours: small (royal blue); small-medium (purple); medium-large (orange); large (red); and, preovulatory (green).

Metalloids

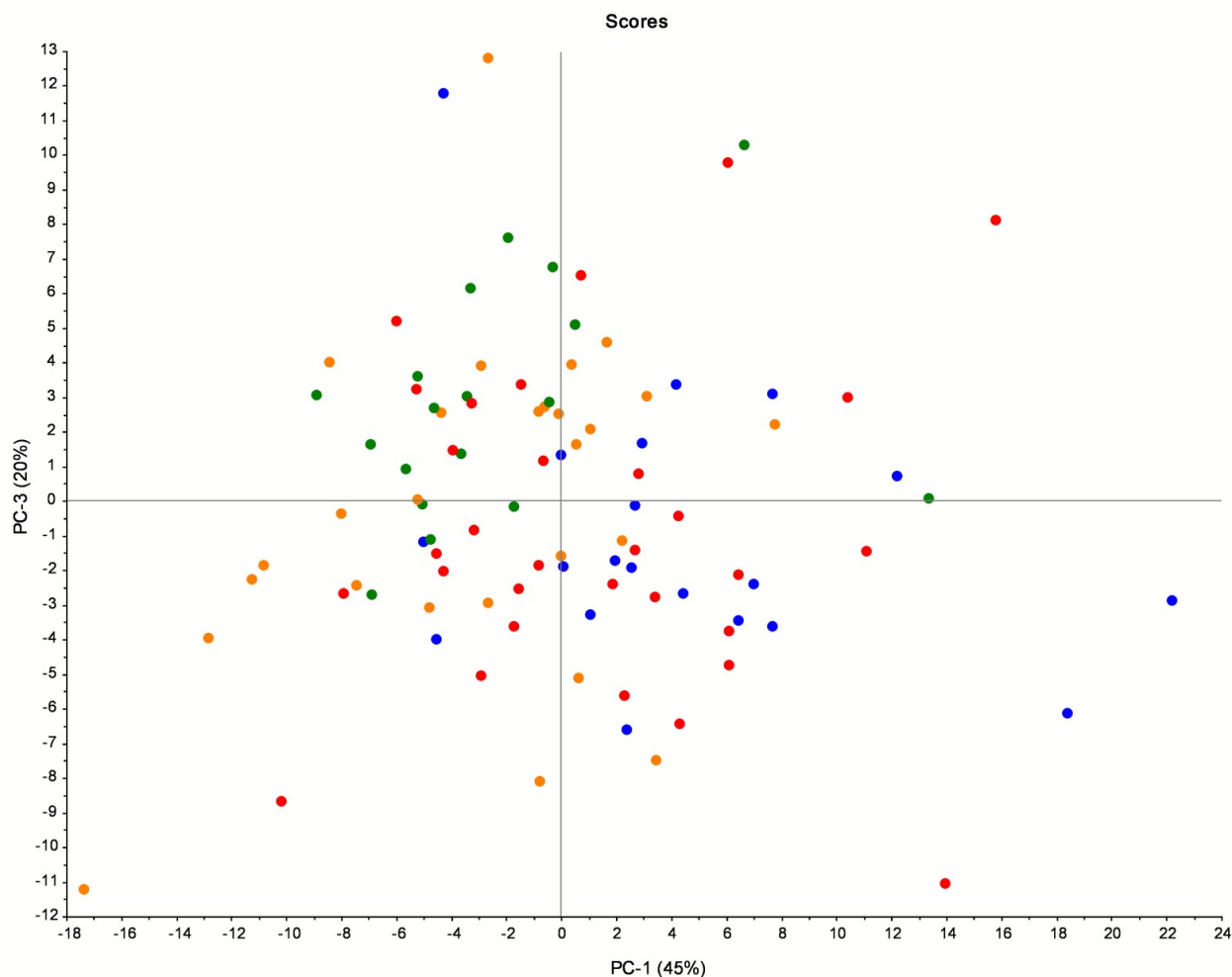


Fig. 6 PC3 versus PC1 scores plot derived from average elemental concentrations data. Follicle health statuses are highlighted by different colours: healthy (green); early atretic (orange); atretic (red); and, regressed (blue).

An unconventional depiction of PC4 versus PC1 (Fig. 5) supports a conclusion that was drawn from the one-way ANOVA testing of size-grouped follicles; large follicles, irrespective of their health status, tend to be dissimilar to follicles of all other sizes. From a PCA perspective Se loads almost entirely onto PC4 and thus it is the differences in Se expression which separates these follicles from the majority of the cohort. The relationship of Se presence with the size of the follicle suggests an important biological role with the most likely function being that the selenoproteins are providing a defence against oxidative stress and inevitable atresia or damage to DNA in the oocyte.¹⁴ As presented by Ceko *et al.* glutathione peroxidase 1 (GPx1) is the selenoprotein that gives rise to the Se imaged through XRF.

It would be remiss to ignore the fact that although the majority of outlier follicles are large and preovulatory in Fig. 5 (quadrants one and two), there are three small and one small-medium follicle lying within this region. One conclusion would be to simply assign these follicles as

anomalous given that in the case of the small follicles they represent less than 6% of the small follicle population, or perhaps the wrong size classification was given if the H&E only showed the edge of the follicle as opposed to its maximum diameter. An alternative hypothesis would be that these follicles may in fact be destined for dominant follicle selection given that their trace element content is closely aligned with all other follicles that have reached this stage of growth.

Fig. 6 highlights the stage classification of all 97 follicles included in this PC analysis. By plotting PC3, which was most heavily loaded onto by Zn (more specifically the Zn that was anticorrelated with the Fe/Zn of PC2) against PC1 (Br) one notices a tendency for the healthy and early atretic follicles to cluster in the first quadrant. One can hypothesise that with a larger data set and perhaps more elements included in the analysis, the follicle group clustering would become more pronounced.

Although this is the first study to investigate the differences in trace elemental concentration of bovine ovarian follicle tissue, other authors have explored the differences in trace element concentration in follicular fluid to examine whether relationships between follicle size and trace element content were evident. In a study of small and large antral follicles in goat ovaries by atomic absorption spectrometry it was found that the concentrations of Zn and Fe were significantly higher in small follicles, while the levels of Cu did not differ significantly between groups.¹⁸ Sadeghi and colleagues investigated the trace element content of follicular fluid in follicles derived from bovine ovaries but found no statistically significant difference between size groups (small, medium and large) for Cu, Fe, Zn and Se.¹⁹ Iodine and manganese however were significantly different across the groups and thus they concluded that the levels of trace elements in follicular fluid were related to follicle size in dairy cows.

With regard to XRF imaging of animal-derived biological tissue, only a handful of studies have previously employed this technique for quantitative means, with many studies choosing to report concentrations in relative terms.^{20,21,22,23,24} Malinouski *et al.* acknowledged that although alternative techniques such as Inductively Coupled Plasma Mass Spectrometry (ICP-MS) can quantify trace elements in various organs, this technique does not address the element's spatial distribution within cells and tissues, which is perhaps the most useful information.²² Combination with a laser ablation apparatus does allow spatial information to be collected using ICP-MS, however the poorer combined spatial resolution and sensitivity of the method compared to synchrotron-based XRF imaging means that a study of the size reported here would be infeasible.

It is commonplace for authors to report localisation of elements to specific structures in the form of qualitative elemental distribution maps, and describe elemental co-localisations, but many err on the side of caution when it comes to providing quantitative data. A handful of authors however do present validation of their quantitative XRF data either by using an alternative analytical technique,^{25,26} or imaging a standard reference material in conjunction with their tissue of interest.^{27,28} James and colleagues show how well XRF derived trace element concentrations in the hippocampus of a rat brain compare with values obtained by Inductively Coupled Plasma Optical Emission Spectroscopy (ICP-OES). They report percentage differences not exceeding 11%.²⁵ In an attempt to render our data comparable with the trace elemental content of follicles which may be captured by alternative analytical techniques (ICP-OES, ICP-MS, electron paramagnetic resonance (EPR) spectroscopy), we chose to present the data as ppm estimates.

Critique of the analysis

Data were collected over two separate beamtime experiments with the follicle measurement technique being modified partway through (as detailed in the *Classification of follicles* section). This may have led to erroneous determination of the size (diameter) of the follicles as a

follicle measured post embedding and dissection is likely to be smaller than it was *in vivo* due to the drainage of follicular fluid.

Two types of scans were collected at the beamline with the vertical step sizes being 6 μm and 2 μm for the coarse and fine scans, respectively. Taking into consideration the beam size of 2 μm , the coarse scans would have been significantly undersampled in the vertical direction. Owing to the longer dwell time, the fine scan also would have captured more detail and thus produced an elemental distribution map of higher resolution. Due to time constraints at the beamline the majority of follicles were captured as coarse scans. To maintain consistency the quantitative data presented in this research stems primarily from the coarse scans excluding one case where the fit was so poor that the fine scan was used as a substitute. Ultimately the user-selected ratio of beam size to step size could lead to different quantitative results. As discussed in the *Statistical analysis of data* section, it was initially envisaged that the Cu results would be included here. The ANOVA results however, combined with the actual elemental distribution maps which showed no structural accumulation of Cu, led to this expectation being reversed. Additionally, 85% of follicles contained Cu at levels less than or equal to the background concentrations. There were a handful of sections depicting high Ti with the pattern of expression suggesting metallic contamination during the cryostat sectioning process. For this reason this element was not considered for subsequent analysis.

With regard to selecting the follicular ROIs, it was challenging to ascertain what portion of the follicle should be analysed and how some form of consistent analysis could be employed across sections to allow valid comparisons. Initially the possibility of analysing a region that represented 25% of the total follicle wall was considered. In many cases however only a tiny portion of the follicle was captured in the scan, possibly representing less than 25%, and thus it was decided that in all cases a region of the follicle wall would be selected as long as the tissue appeared unique to that follicle (based on comparison with the adjacent H&E stain) and independent of any other structures. To clarify, there were many scenarios where a cluster of follicles appeared in a scan and care was taken to position the image region analysis tool on an area exclusively associated with the follicle in question (i.e. no shared follicle edges and a tighter region which aimed to avoid communal stromal tissue).

With regard to the health status grouping producing statistically significant results for only a handful of the Br and Zn comparisons, it should be acknowledged that a great deal of subjectivity exists when differentiating between a healthy and an early atretic follicle, as well as those follicles in late atresia versus regressing. This subjectivity could ultimately lead to overlap between the follicle groups and thereby lead to such elements as Fe having no statistical differences despite the general trend being for this element's levels to steadily decrease from early atretic though to regressed follicles.

Conclusions

In this research XRF imaging has been used for the first time in mammalian ovaries to quantitatively compare the concentrations of Cu, Fe, Zn, Se and Br in follicles of different sizes and at different stages of health. Cu, Fe, Zn and Se all play an important role in female reproductive function with deficiency studies highlighting the negative effects on ovarian function and follicular development. Subregions of 97 imaged antral follicles were analysed within GeoPIXE v6.4g and the average elemental concentrations of the granulosa and thecal cell layers extracted for comparison. One-way ANOVA indicated statistically significant elemental differences amongst the cohort of 97 follicles when they were categorised according to size or health status. Post hoc t-testing showed statistically significant elemental differences existed between the following follicle pairs: early atretic versus regressed for Fe; small versus large, and small versus preovulatory follicles for Se; and healthy versus regressed, and early atretic versus regressed for Br ($p < 0.005$, Bonferroni corrected). PCA highlighted that when follicles were divided into size groups the main element differentiating the large follicles from their smaller counterparts was Se. With regard to stage differentiated antral follicles the elemental intricacies are more complex with PCA suggesting that the relationship between Br and Zn (specifically Zn uncorrelated with Fe) sets the healthy and early atretic follicles aside from the remaining categories. This research provides insights into the challenges of quantitative XRF and more importantly highlights how this innovative technique can be used to differentiate between biological structures on trace element grounds alone. It is envisaged that a larger data set, a fixed follicle measurement protocol, and the addition of diseased state tissue would provide further insights into the biochemistry of this organ.

Acknowledgements

The authors wish to acknowledge: T&R Pastoral for their donation of bovine ovaries; Wendy Bonner for her collection and sectioning of the tissues; Claire Weekley for her support during the XFM beamline experiments; the XFM beamline team including David Paterson, Martin de Jonge, Daryl Howard, Simon James and Kathryn Spiers for the research that was undertaken at the Australian Synchrotron, Victoria, Australia; Chris Ryan for his technical support with GeoPIXE data processing; and, the Australian Research Council (DP0985807, DP0984722, DP140100176) and National Health and Medical Research Council for funding.

Notes and references

^a Department of Chemistry, The University of Adelaide, SA, 5005, Australia

^b Discipline of Obstetrics and Gynaecology, School of Paediatrics and Reproductive Health, Robinson Research Institute, University of Adelaide, SA, Australia

1. N. Hatzirodos, K. Hummitzsch, H. F. Irving-Rodgers, M. L. Harland, S. E. Morris and R. J. Rodgers, Transcriptome profiling of granulosa cells from bovine ovarian follicles during atresia, *BMC Genomics*, 2014, **15**, 40.
2. M. Tsai-Turton and U. Luderer, Opposing effects of glutathione depletion and follicle-stimulating hormone on reactive oxygen species and apoptosis in cultured preovulatory rat follicles, *Endocrinology*, 2006, **147**, 1224-1236.
3. J. Singh, G. P. Adams and R. A. Pierson, Promise of new imaging technologies for assessing ovarian function, *Anim. Reprod. Sci.*, 2003, **78**, 371-399.
4. M. J. Pushie, I. J. Pickering, M. Korbas, M. J. Hackett and G. N. George, Elemental and Chemically Specific X-ray Fluorescence Imaging of Biological Systems, *Chem. Rev.*, 2014, **114**, 8499-8541.
5. R. S. Bedwal and A. Bahuguna, Zinc, Copper and Selenium in Reproduction, *Experientia*, 1994, **50**, 626-640.
6. S. K. Taneja and R. Kaur, Pathology of ovary, uterus, vagina and gonadotrophs of female mice fed on Zn-deficient diet, *Indian J. Exp. Biol.*, 1990, **28**, 1058-1065.
7. M. Yaman, G. Kaya and M. Simsek, Comparison of trace element concentrations in cancerous and noncancerous human endometrial and ovary tissues, *Int. J. Gynecol. Cancer*, 2007, **17**, 220-228.
8. Y. Q. Li, X. X. Cao, B. Bai, J. N. Zhang, M. Q. Wang and Y. H. Zhang, Severe Iron Deficiency Is Associated with a Reduced Conception Rate in Female Rats, *Gynecol. Obstet. Invest.*, 2014, **77**, 19-23.
9. C. Michos, V. Kalfakakou, S. Karkabounas, D. Kiortsis and A. Evangelou, Changes in copper and zinc plasma concentrations during the normal menstrual cycle in women, *Gynecol. Endocrinol.*, 2010, **26**, 250-255.
10. A. T. Grazul-Bilska, J. S. Caton, W. Arndt, K. Burchill, C. Thorson, E. Borowczyk, J. J. Bilski, D. A. Redmer, L. P. Reynolds and K. A. Vonnahme, Cellular proliferation and vascularization in ovine fetal ovaries: effects of undernutrition and selenium in maternal diet, *Reproduction*, 2009, **137**, 699-707.
11. M. Grabek, Z. Swies and A. Borzecki, The influence of selenium on the reproduction of rats, *Annales Universitatis Mariae Curie-Skłodowska. Sectio D: Medicina*, 1991, **46**, 103-105.
12. M. J. Ceko, K. Hummitzsch, N. Hatzirodos, W. Bonner, S. A. James, R. J. Rodgers and H. H. Harris, Distribution and speciation of bromine in mammalian tissue and fluids by X-ray fluorescence microspectroscopy and X-ray absorption spectroscopy, *Metalloomics*, 2015, DOI:10.1039/C4MT00338A.
13. A. S. McCall, Christopher F. Cummings, G. Bhave, R. Vanacore, A. Page-McCaw and Billy G. Hudson, Bromine Is an Essential Trace Element for Assembly of Collagen IV Scaffolds in Tissue Development and Architecture, *Cell*, 2014, **157**, 1380-1392.

14. M. J. Ceko, K. Hummitzsch, N. Hatzirodos, W. M. Bonner, J. B. Aitken, D. L. Russell, M. Lane, R. J. Rodgers and H. H. Harris, X-Ray fluorescence imaging and other analyses identify selenium and GPX1 as important in female reproductive function, *Metallomics*, 2015, **7**, 71-82.
15. C. G. Ryan, Quantitative trace element imaging using PIXE and the nuclear microprobe, *Int. J. Imag. Syst. Tech.*, 2000, **11**, 219-230.
16. C. G. Ryan, Developments in dynamic analysis for quantitative PIXE true elemental imaging, *Nucl. Instrum. Meth. B.*, 2001, **181**, 170-179.
17. M. J. Ceko, K. Hummitzsch, W. M. Bonner, J. B. Aitken, K. M. Spiers, R. J. Rodgers and H. H. Harris, Localization of the trace elements iron, zinc and selenium in relation to anatomical structures in bovine ovaries by X-ray fluorescence imaging., *Microsc. Microanal.*, 2015, DOI:10.1017/S1431927615000380.
18. P. R. Nandi, B. K. Mehta and D. Sengupta, Changes in concentration of minerals in follicular fluid of growing follicles, *Exploratory Animal and Medical Research*, 2012, **2**, 166-169.
19. S. Sadeghi and N. M. Kor, Trace elements in ovarian follicular fluid related to follicle size in dairy cows, *Online Journal of Veterinary Research*, 2013, **17**, 490-495.
20. R. V. Hyne, R. M. Mann, C. T. Dillon, M. D. de Jonge, D. Paterson and D. L. Howard, Secondary vitellogenesis persists despite disrupted fecundity in amphipods maintained on metal-contaminated sediment: X-ray fluorescence assessment of oocyte metal content, *Ecotox. Environ. Safe.*, 2013, **93**, 31-38.
21. R. Evens, K. A. C. De Schampelaere, B. De Samber, G. Silversmit, T. Schoonjans, B. Vekemans, L. Balcaen, F. Vanhaecke, I. Szaloki, K. Rickers, G. Falkenberg, L. Vincze and C. R. Janssen, Waterborne versus Dietary Zinc Accumulation and Toxicity in *Daphnia magna*: a Synchrotron Radiation Based X-ray Fluorescence Imaging Approach, *Environ. Sci. Technol.*, 2012, **46**, 1178-1184.
22. M. Malinouski, S. Kehr, L. Finney, S. Vogt, B. A. Carlson, J. Seravalli, R. Jin, D. E. Handy, T. J. Park, J. Loscalzo, D. L. Hatfield and V. N. Gladyshev, High-Resolution Imaging of Selenium in Kidneys: A Localized Selenium Pool Associated with Glutathione Peroxidase 3, *Antioxid. Redox Signal.*, 2012, **16**, 185-192.
23. B. F. G. Popescu, M. J. George, U. Bergmann, A. V. Garachtchenko, M. E. Kelly, R. P. E. McCrea, K. Luning, R. M. Devon, G. N. George, A. D. Hanson, S. M. Harder, L. D. Chapman, I. J. Pickering and H. Nichol, Mapping metals in Parkinson's and normal brain using rapid-scanning x-ray fluorescence, *Phys. Med. Biol.*, 2009, **54**, 651-663.
24. C. M. Weekley, J. B. Aitken, S. Vogt, L. A. Finney, D. J. Paterson, M. D. de Jonge, D. L. Howard, P. K. Witting, I. F. Musgrave and H. H. Harris, Metabolism of Selenite in Human Lung Cancer Cells: X-Ray Absorption and Fluorescence Studies, *J. Am. Chem. Soc.*, 2011, **133**, 18272-18279.
25. S. A. James, D. E. Myers, M. D. de Jonge, S. Vogt, C. G. Ryan, B. A. Sexton, P. Hoobin, D. Paterson, D. L. Howard, S. C. Mayo, M. Altissimo, G. F. Moorhead and S. W. Wilkins, Quantitative comparison of preparation methodologies for x-ray fluorescence microscopy of brain tissue, *Anal. Bioanal. Chem.*, 2011, **401**, 853-864.
26. W. L. Zheng, H. Nichol, S. F. Liu, Y. C. N. Cheng and E. M. Haacke, Measuring iron in the brain using quantitative susceptibility mapping and X-ray fluorescence imaging, *Neuroimage*, 2013, **78**, 68-74.
27. M. Szczerbowska-Boruchowska, Sample thickness considerations for quantitative X-ray fluorescence analysis of the soft and skeletal tissues of the human body - theoretical evaluation and experimental validation, *X-Ray Spectrom.*, 2012, **41**, 328-337.
28. Z. Y. Zhang, N. Q. Liu, F. L. Li, J. Zhang, H. Zhu, C. Qin, Z. Y. Zou and X. W. Tang, Characterization of Fe, Cu and Zn in organs of PDAPP transgenic mice by XRF spectrometry, *X-Ray Spectrom.*, 2006, **35**, 253-256.